

Semantic-guided Automatic Natural Image Matting with Trimap Generation Network and Light-weight Non-local Attention

Yuhongze Zhou,¹ Liguang Zhou,^{2,3} Tin Lun Lam,^{2,3} * Yangsheng Xu^{2,3}

¹ McGill University

² The Chinese University of Hong Kong, Shenzhen

³ Shenzhen Institute of Artificial Intelligence and Robotics for Society

yuhongze.zhou@mail.mcgill.ca, {liguangzhou@link., tllam@, ysxu@}cuhk.edu.cn

Abstract

Natural image matting aims to precisely separate foreground objects from background using alpha matte. Fully automatic natural image matting without external annotation is challenging. Well-performed matting methods usually require accurate labor-intensive handcrafted trimap as extra input, while the performance of automatic trimap generation method of dilating foreground segmentation fluctuates with segmentation quality. Therefore, we argue that how to handle trade-off of additional information input is a major issue in automatic matting. This paper presents a semantic-guided automatic natural image matting pipeline with Trimap Generation Network and light-weight non-local attention, which does not need trimap and background as input. Specifically, guided by foreground segmentation, Trimap Generation Network estimates accurate trimap. Then, with estimated trimap as guidance, our light-weight Non-local Matting Network with Refinement produces final alpha matte, whose trimap-guided global aggregation attention block is equipped with stride downsampling convolution, reducing computation complexity and promoting performance. Experimental results show that our matting algorithm has competitive performance with state-of-the-art methods in both trimap-free and trimap-needed aspects.

Introduction

Image matting is a popular image editing task which attempts to extract perfect foreground object mask, i.e. alpha matte, from background. Matting problem can be formulated in a general mathematical manner. An image I can be defined as a combination weight of alpha matte α , foreground F , and background B image as follows:

$$I = \alpha F + (1 - \alpha)B, \quad (1)$$

where the RGB color I is known, but F , B and α are unknown. That is to say, matting attempts to solve 7 unknown variables with only 3 variables provided. Therefore, most compelling matting methods usually require a handcrafted trimap for region constrain to reduce complexity and assist matte estimation, which makes fully-automatic natural image matting such an appealing task to explore.

Let us recap recent learning-based image matting approaches and their pros and cons. Learning-based image

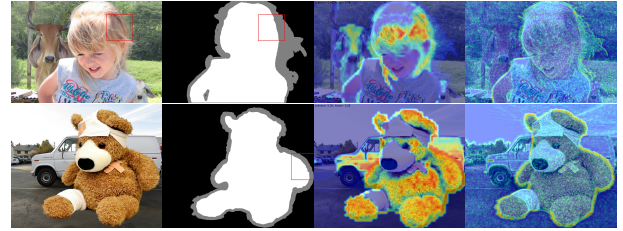


Figure 1: The visualization of our attention block. From left to right, image, trimap, global attention weight map of given query patch marked by red box, and reconstructed alpha feature of attention block.

matting can be divided into three primary categories, i.e. background-required (Qian and Sezan 1999; Sengupta et al. 2020), only-image (Qiao et al. 2020; Zhang et al. 2019; Wei et al. 2021) input, and trimap-needed (Cho, Tai, and Kweon 2016; Xu et al. 2017; Lutz, Amliantitis, and Smolic 2018; Lu et al. 2019; Tang et al. 2019; Li and Lu 2020; Sun, Tang, and Tai 2021; Dai, Lu, and Shen 2021).

Recently, novel background matting (Sengupta et al. 2020; Lin et al. 2021) is proposed, but it cannot resist interference of shadows or complex light condition. For algorithms requiring only single image (Qiao et al. 2020; Zhang et al. 2019), results on generic objects are far from practical expectations. Although human matting, one branch of trimap-free matting, has achieved impressive performance (Shen et al. 2016; Chen et al. 2018; Liu et al. 2020; Ke et al. 2020), human is regarded as such a specific domain and salient object that it is easy for network to capture foreground/background discrepancy. So does animal image matting (Li et al. 2020).

For trimap-needed matting, its accuracy is paramount, which gives the credit to auxiliary trimap. The trimap provides deterministic foreground, unknown, and background regions of image, which narrows down matte estimation to unknown region and reset pixel values of known region. Besides, the manual creation of trimap is painstaking, which diminishes its application potential. Hence, trimap quality is one significant factor that can affect matting performance. One possible workaround is a general automatic trimap generation method, that is, target foreground items are roughly

*Corresponding Author

extracted by semantic segmentation and then processed by image dilation/erosion. Regarding this way, semantic segmentation quality has a dominant influence on corresponding trimap, similar to what trimap is to matte.

From the above-mentioned problems, it is obvious that **trimap-needed matting (resp., mentioned trimap generation method) has a trimap (resp., foreground segmentation) quandary**. Although previous methods attempt to solve these puzzles, they mainly focus on single-category matting by exploring refining trimap to boost matting results (Shen et al. 2016; Cai et al. 2019), employing implicit trimap to assist human/animal matting without trimap input (Chen et al. 2018; Zhang et al. 2019; Li et al. 2020), and coupling coarse annotated data with fined one to promote human matting (Liu et al. 2020), which **are hard to generalize to comprehensive data and usually require salient single-category object**.

Considering forementioned issues, we argue that how to find a balance between extra knowledge and matte accuracy is a critical cornerstone for automating natural image matting. Therefore, we disentangle automatic matting into trimap and alpha estimation subtasks as workaround. Different from all past attempts, we aim to generalize trimap-free matting more properly to comprehensive data. We propose a semantic-guided trimap-free matting approach, which consists of Trimap Generation Network and light-weight Non-local Matting Network with Refinement Module. Coarse foreground segmentation provides additional semantic information and can help network capture rough location and shape of target object, which can be easily obtained by salient/segmentation models. Then, Trimap Generation Network employs coarse foreground segmentation as guidance to estimate a proper trimap. This estimated trimap serves as guidance for matting network and also buffer for negative trimap quality chain reaction. Our proposed light-weight non-local attention block utilizes stride downsampling convolution to reduce similarity computation cost and rearranges alpha feature by propagating the global pixel-to-pixel relationship of image feature on an explicit fashion. Refinement module with fusion techniques bridges two main components together to produce high-quality alpha matte without trimap and background as input. Extensive experiments show that our matting pipeline has superior performance and comparable with other state-of-the-art methods on the Composition-1k testset, alphamattng.com benchmark, and Distinctions-646 testset. To demonstrate real-world application capability of our pipeline, we conduct real data adaption by finetuning our framework on real imagery data and user study for verification. The sufficient ablation analysis also justifies Trimap Generation Network to be segmentation fault-tolerance and qualified for automatic matting task.

The main contribution of this work is threefold. First, we propose a novel two-stage trimap-free automatic natural image matting approach boosted by coarse foreground segmentation and our light-weight non-local attention, which is on a par with the state-of-the-art matting in trimap-needed and trimap-free respects. Our proposed method finds a trade-off between additional information and performance. **We believe that this matting architecture should**

be more rational trimap-free matting framework, which has comprehensive integration ability with other semantic segmentation/salient object detection/matting approaches to better solve automatic natural image matting. Second, we propose Trimap Generation Network to predict the possibility of each pixel belonging to foreground/background/unknown areas, which can not only better capture semantic information, but also provide accurate trimap with defective segmentation as input. Third, our light-weight attention layer not only reduces computational complexity but also maintains effective performance.

Related Works

Natural Image Matting: Traditional image matting can be roughly classified into sampling-based (Chuang et al. 2001; Wang and Cohen 2005, 2007; Gastal and Oliveira 2010; He et al. 2011; Shahrian et al. 2013; Aksoy, Ozan Aydin, and Pollefeys 2017) and propagation-based (Chen, Li, and Tang 2013; Grady et al. 2005; Lee and Wu 2011; Levin, Lischinski, and Weiss 2007; Levin, Rav-Acha, and Lischinski 2008; Sun et al. 2004) approaches, which usually require trimap as additional input. Recently, matting techniques using deep learning have shown increasingly prominent performance, which can be categorized into trimap-needed (Cho, Tai, and Kweon 2016; Xu et al. 2017; Lutz, Amplianitis, and Smolic 2018; Lu et al. 2019; Tang et al. 2019; Li and Lu 2020; Yu et al. 2020; Sun, Tang, and Tai 2021; Dai, Lu, and Shen 2021), background-required (Qian and Sezan 1999; Sengupta et al. 2020; Lin et al. 2021) and only-image (Aksoy et al. 2018; Zhang et al. 2019; Qiao et al. 2020; Wei et al. 2021) input. After Cho et al. (Cho, Tai, and Kweon 2016) introduce deep neural networks into image matting task, Xu et al. (Xu et al. 2017) propose a deep neural network matting solution with a comprehensive matting database which has promoted research progress significantly. Lutz et al. (Lutz, Amplianitis, and Smolic 2018) explore matting task with a generative adversarial framework. Then, appealing matting results are achieved by Lu et al. (Lu et al. 2019) and Tang et al. (Tang et al. 2019). Subsequently, a state-of-the-art matting method with guided contextual attention is proposed, which not only simulates information flow of affinity-based methods but also models matting in a view of image inpainting (Li and Lu 2020). Given an image, background, and soft segmentation, background matting (Sengupta et al. 2020) is adapted to real human data and obtains appealing estimation but is not robust to images with shadow or under complex light conditions. Since trimap-needed matting algorithm usually requires high-quality time-consuming hand-made trimap, a few works are attempting to take only image as input and produce matte (Zhang et al. 2019; Qiao et al. 2020). However, these trimap-free methods are not capable of producing comparable quality matte.

Attention Mechanism: Attention mechanism has been widely utilized in deep learning tasks like machine translation (Vaswani et al. 2017; Tang et al. 2018), image classification (Mnih et al. 2014; Jetley et al. 2018), video classification (Wang et al. 2018), and semantic segmentation (Fu et al. 2019; Huang et al. 2019). The self-attention block is introduced to transformer and contributes to each position

of output by referring to every position of input (Vaswani et al. 2017). Similarly, Wang et al. (Wang et al. 2018) propose non-local attention to acquire long-range contextual information and promote video classification tasks. Instead of capturing long-term dependencies in sequences, attention has shown its superiority in image matting (Li and Lu 2020; Qiao et al. 2020; Yu et al. 2020), by making matting network capture structural pixel-to-pixel dependencies of image that can deepen semantic understanding of network. Li et al. (Li and Lu 2020) simulate non-local attention by convolution and deconvolution to enhance alpha matte estimation. Qiao et al. (Qiao et al. 2020) use channel/spatial-wise attention to filter out noise from hierarchical appearance cues and boost alpha mattes. Yu et al. (Yu et al. 2020) introduce three non-local attentions to propagate each trimap region of context patches to corresponding region of query patches. However, our approach leverages only one attention layer and has better matting performance.

Trimap Generation: Automatic trimap generation, which is popular in traditional matting (Wang et al. 2007; Hsieh and Lee 2013; Gupta and Raman 2016; Chen et al. 2020), usually contains two steps: binary segmentation for foreground/background separation and image erosion/dilation. These methods mainly differentiate in how to obtain segmentation. For example, Wang et al. (Wang et al. 2007) leverage depth information to compute segmentation; Gupta et al. (Gupta and Raman 2016) combine salient object detection with superpixel analysis for segmentation; Hsieh et al. (Hsieh and Lee 2013) use graph cuts for foreground extraction; Chen et al. (Chen et al. 2020) require user to indicate foreground/background by a few clicks and apply one-shot learning for binary mask prediction. Recently, neural networks have been utilized to generate implicit trimap for human matting automation (Shen et al. 2016; Chen et al. 2018).

Approach

We decompose our trimap-free matting approach into **Trimap Generation Network (Net-T)** and **light-weight Non-local Matting with Refinement (Net-M)**. With rough foreground segmentation (Yang et al. 2019; Chen et al. 2017) as additional indicator, Net-T understands target object shape and its relation with surroundings to perform accurate pixel-wise classification among foreground/background/unknown regions. Net-M utilizes RGB image and output of Net-T to estimate alpha matte. The overview of our proposed matting framework is illustrated in Fig. 4.

Trimap Generation Network (Net-T)

Net-T conducts a 3-class semantic segmentation task, where the input of Net-T is the concatenation of a cropped RGB image and a 2-channel one-hot soft foreground segmentation, and the output of Net-T is a 3-channel feature map indicating the possibility that each pixel is assigned to each of 3 classes. We utilize a modified Deeplabv3 (Chen et al. 2017) as the encoder by adjusting the input channel size and taking the first two channel weights of *conv_1* of the pre-trained ResNet-50 as the weight for 2-channel segmentation.

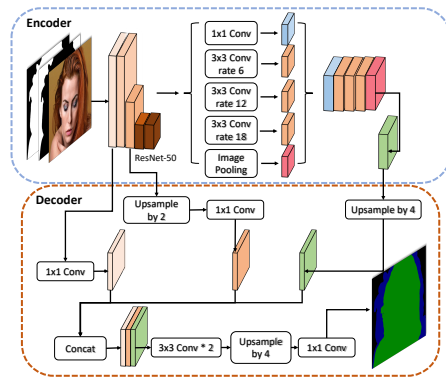


Figure 2: Trimap Generation Network (Net-T)

Instead of using its original decoder, we propose our own decoder to reconstruct semantic information, as illustrated in Fig. 2. The dropout layer by 0.5 factor is first applied to high-level encoder feature, followed by a four-time bilinearly upsampling. Then, instead of directly adopting high-level encoder feature for final classification, we aggregate it with low and middle-level features of encoder to enrich the decoding process and make network pay attention to image appearance and less dependent on segmentation input. And the swapped order of upsampling and final convolution makes classification more fine-grained. Due to these careful designs, Net-T can be tolerant for inaccuracy of foreground segmentation.

Non-local Matting with Refinement (Net-M)

We adopt popular U-Net structure (Ronneberger, Fischer, and Brox 2015; Li and Lu 2020) as the main architecture, illustrated in Fig. 4.

light-weight Non-local Matting (NLM): Traditional matting methods usually estimate unknown pixels by investigating color similarity of unknown/known areas, and formulating transition pixels as weight combination of relevant foreground/background pixels based on certain criteria. Inspired by startling capability of attention (Li and Lu 2020), we design a light-weight non-local attention block to model classic matting in order to promote alpha feature learning and speed up training. Fig. 3 shows details of our light-weight Non-local attention block. Instead of simulating similarity computation by a convolution between unknown region and kernels reshaped from image feature (Li and Lu 2020), we explicitly calculate similarity between each pixel and the rest via embedded dot-product in the transformed image feature space with scaled softmax normalization. And then this pixel-to-pixel relation is employed to reconstruct the original alpha feature A as A' :

$$A'_{x,y} = A_{x,y} + \mathbf{W} \left(\sum_{\forall x',y'} f(I_{x,y}, I_{x',y'}) g'(A_{x',y'}) \right), \quad (2)$$

$$f(I_{x,y}, I_{x',y'}) = \text{softmax}(w(U, K, x, y) \frac{\theta(I_{x,y})^T \phi'(I_{x',y'})}{\sqrt{d/2}}), \quad (3)$$

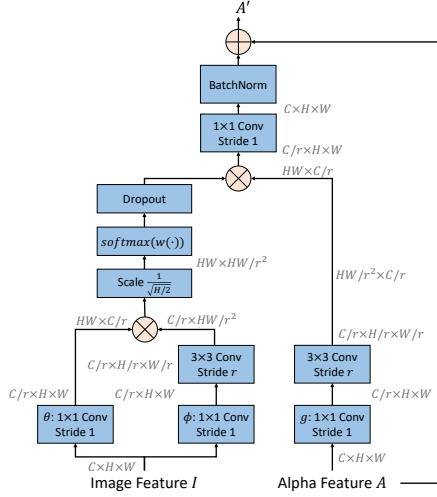


Figure 3: Light-weight Non-local Attention Block. The size of feature maps are shown. “ \oplus ” means element-wise sum, “ \otimes ” denotes matrix multiplication and r is the downsample ratio. The softmax operation is performed on each row.

$$w(U, K, x, y) = \begin{cases} \text{clip}(\sqrt{|U|/|K|}) & I_{x,y} \in U, \\ \text{clip}(\sqrt{|K|/|U|}) & I_{x,y} \in K, \end{cases}, \quad (4)$$

$$\text{clip}(x) = \min(\max(x, 0.1), 10), \quad (5)$$

where I refers to image feature map, $I_{x,y}$ is pixel value at the position (x, y) of I , $g'(\cdot)$ and $\phi'(\cdot)$ denote embedded linear transformation and downscale operation, d is the dimension of original feature map, U is the unknown region, $K = I - U$ and \mathbf{W} is the learnable weight matrix. Considering the barrier of high computational cost of dot-product calculation, we choose stride convolutions to downscale features which can not only maintain less information loss than pooling or interpolation does, but also speed up training and prevent gradient explosion/vanishing. The downscale ratio of r is set to 4 in our experiments. Dropout is applied to prevent overfitting, and the residual summation is to stable the training. We assume that the attention block escorts the encoder to understand unknown areas and summation connections between encoder and decoder open the information communication gate to assist transition reconstruction in the decoder.

Refinement Module: Refinement technique has been applied to salient object detection and semantic segmentation (Deng et al. 2018; Amirul Islam, Kalash, and Bruce 2018), and shown impressive performance. There exists similarity between salient object detection, which can be considered as coarse alpha matte estimation using only RGB image, and image matting, a regression version of 2-class semantic segmentation. Based on this insight, we introduce refinement module to refine the predicted coarse alpha α_{coarse} by learning the residuals $\alpha_{residual}$ between the coarse alpha and ground truth as $\alpha_{refined} = \alpha_{coarse} + \alpha_{residual}$.

Loss Function The cross-entropy loss is for 3-class classification in Net-T. For Net-M, its training loss L is defined as

the summation over losses of coarse and refined alpha estimations, $L = L_{coarse.\alpha} + L_{refined.\alpha}$. To obtain high-quality alpha matte, we employ the summation of alpha prediction loss L_{alpha} and alpha hard mining loss L_{hard} for both coarse and refined alpha prediction. The alpha prediction loss is defined as the absolute difference between the ground truth and predicted alpha, $L_{alpha} = \frac{1}{|\mathcal{M}|} \sum_{i \in \mathcal{M}} |\hat{\alpha}_i - \alpha_i|$, where \mathcal{M} refers to the unknown region. Since difficulty degree of each alpha pixel for the network to learn varies a lot and indiscriminately calculating loss on unknown region might misguide training process, we introduce hard mining loss (Shrivastava, Gupta, and Girshick 2016; Xu et al. 2019). The hard mining loss calculates the absolute difference between the predicted and groundtruth alpha, sort all pixels, and pick the top p percent of the largest error pixels as hard samples to automatically guide model to focus more on hard alpha region. The hard mining loss is defined as $L_{hard} = \frac{1}{|\mathcal{HM}|} \sum_{i \in \mathcal{HM}} |\hat{\alpha}_i - \alpha_i|$, where \mathcal{HM} means the region that contains hard samples, $\hat{\alpha}_i, \alpha_i$ indicate the predicted and ground-truth alpha at position i and $p = 50$ in our experiments.

Experiment Settings and Results

Experiment Settings

We train Net-T and Net-M separately and then test the whole net jointly with fusion techniques (Chen et al. 2018) (Joint Inference).

Net-T: Here is random soft foreground segmentation input generation process.¹ Random trimap is first produced by random erosion on both foreground and background of alpha ranging from 1 to 29 pixels (Li and Lu 2020). The unknown and foreground areas of random trimap is considered as foreground of random *initial segmentation*. Then, random soft segmentation is generated by eroding and dilating random *initial segmentation* sequentially with random number of pixels ranging from 1 to 59 and followed by a random Gaussian Blur (Sengupta et al. 2020). To obtain *synthesized ground-truth trimap* for supervision, we apply 15-pixel erosion on both foreground and background of alpha. Image patches are randomly cropped from input images and then resized to 512×512 . We train Net-T for 129,300 iterations with 10 batch size. The learning rate is initialized to 0.001 and adjusted every iteration.

Net-M: We follow the same data processing and augmentation procedure as GCA-Matting (Li and Lu 2020). Net-M is trained for 400,000 iterations with 20 batch size and $L_{coarse.\alpha} + L_{refined.\alpha}$, where unknown region of trimap is \mathcal{M} . The adam optimizer with $\beta_1 = 0.5$ and $\beta_2 = 0.999$ is adopted with initialized learning rate, 4×10^{-4} , plus warmup and cosine decay techniques.

Joint Inference (JI): Joint Inference is Net-T and Net-M collaborative testing by adopting Net-T-predicted trimap as one input of Net-M. Since 1) categories of foreground objects of synthesized matting datasets may not match segmentation datasets; 2) background objects may have the same category as foreground and can also be salient,

¹Please refer to supplementary material for code snapshot.

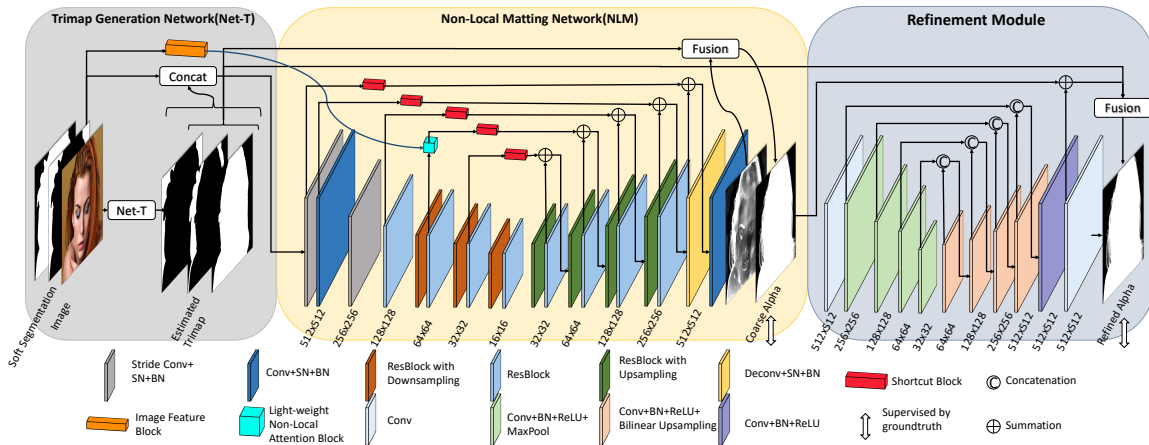


Figure 4: The Overview of our Matting Pipeline. Non-local Matting Network with Refinement Module is Net-M. Net-T and Net-M collaborative testing is Joint Inference. (SN is Spectral Normalization, while BN is Batch Normalization.)

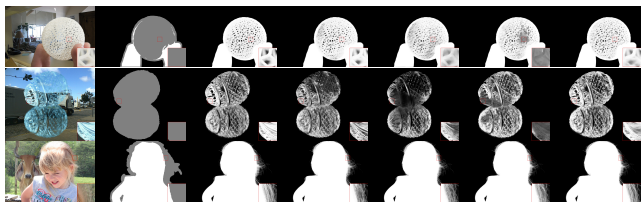


Figure 5: Comparison of visual results of the Composition-1k test dataset of different methods. From left to right, the original image, dataset-provided trimap, GT alpha matte, IM (Lu et al. 2019), CAM (Hou and Liu 2019), GCA (Li and Lu 2020), Net-M

salient/segmentation models may not be suitable for coarse segmentation generation. Therefore, JI setting here is for synthesized datasets (For real data, we provide transfer approach in Real World Human Data part of section 4.2.2.). The soft segmentation input for testing is generated by erosion on *initial segmentation* derived from *synthesized ground-truth trimap* with 20 pixels and followed by a Gaussian Blur. In Fig. 4, raw alpha estimation of Net-M is far away from impressive except unknown region. Hence, we propose two fusion methods to solve this. One is probability-based soft fusion, another is region-based hard fusion. For soft fusion, we use region probabilities estimated by Net-T to reconstruct final alpha α_r from predicted alpha α_p (Chen et al. 2018) as $\alpha_r = (1 - U_p) \frac{F_p}{F_p + B_p} + U_p \alpha_p$, $U_p = 1 - (F_p + B_p)$ and $\alpha_r = F_p + U_p \alpha_p$, where U_p , F_p , and B_p are probabilities of each pixel belonging to unknown/foreground/background regions severally. For hard fusion, we reset trimap-predicted foreground (background) to 255 (0) on predicted alpha.

Experiment Results

Evaluation on trimap We evaluate Net-T and other popular adapted semantic segmentation methods, e.g.

AIM						
Methods	pixAcc	mIoU Bg	mIoU Unk	mIoU Fg	mIoU	
Deeplabv2	93.58	89.81	76.25	63.09	76.38	
Deeplabv3	95.83	91.59	80.25	70.66	80.83	
Net-T	96.41	93.53	82.78	70.64	82.32	
Distinctions-646						
Methods	pixAcc	mIoU Bg	mIoU Unk	mIoU Fg	mIoU	
Deeplabv2	92.58	94.40	72.97	53.82	73.73	
Deeplabv3	95.66	95.11	79.65	65.52	80.09	
Net-T	95.74	96.54	80.83	66.72	81.36	

Table 1: The quantitative comparison of Net-T with adapted Deeplabv3 and Deeplabv2 on Adobe Image Benchmark test-set and Distinctions-646 testset. Bold numbers represent the best scores.

Deeplabv3 and Deeplabv2, on Composite-1k and Distinctions-646 test set, by using pixel classification accuracy (pixAcc) and mean IoU (mIoU) metrics of background(Bg)/unknown(Unk)/foreground(Fg), and three-region-involved. Results in Table 1 shows that trimap segmentation accuracy and mIoU metrics of Net-T are superior to other methods. Considering quantitative results in Table 1 and visual examples presented in Fig. 6, our trimap estimation is competent to mentor Net-M.

Evaluation on alpha matte We follow common evaluation metrics, i.e. Sum of Absolute Differences (SAD), Mean Squared Error (MSE), Gradient error (Grad), and Connectivity error (Conn) to evaluate our approaches on popular matting datasets, including Composition-1k, alphas.matting.com², and Distinctions-646 benchmarks. To validate unlabeled real-world adaption ability of our approach, we choose human as a typical illustration case and conduct a user study for evaluation.

Adobe Image Matting Benchmark (AIM): We follow composition rules Xu et al. proposed (Xu et al. 2017) to syn-

²Please see both quantitative and qualitative results of alphas.matting.com benchmark on supplementary material.

Trimap-needed Evaluation				
Methods	SAD↓	MSE↓	Grad↓	Conn↓
AlphaGAN	52.40	0.0300	38.00	53.00
Deep Image Matting(DIM)	50.40	0.0140	30.00	50.80
IndexNet Matting(IM)	45.80	0.0130	25.90	43.70
AdaMatting	41.70	0.0100	16.80	-
Learning Based Sampling	40.35	0.0099	-	-
Context-Aware Matting(CAM)	35.80	0.0082	17.30	33.20
GCA-Matting(GCA)	35.28	0.0091	16.92	32.53
HDMatt	33.50	0.0073	14.50	29.90
Net-M	29.43	0.0060	12.27	25.80
Net-M w/o L_{hard} (Net-M-nh)	30.75	0.0063	13.12	27.31
Non-local Matting(NLM)	29.77	0.0061	11.96	26.10
Trimap-free Evaluation				
Methods	SAD↓	MSE↓	Grad↓	Conn↓
Late Fusion [†]	58.34	0.011	41.63	59.74
HAttMatting [†]	44.01	0.007	29.26	46.41
JIS w/o refinement(JIS-c) [†]	47.43	0.0055	18.61	41.43
JIS [†]	43.91	0.0054	18.64	39.82
JIH w/o refinement(JIH-c) [†]	42.39	0.0056	18.59	39.87
JIH [†]	41.85	0.0055	18.34	39.42

Table 2: The quantitative results on Composition-1k test-set. (- indicates not given in the original paper. [†] means that all metrics are calculated on the whole image. JIS and JIH means JI with soft and hard fusion respectively. JIS, JIH, -, , and [†] express forementioned meanings through the entire paper.)

Methods	SAD↓	MSE↓	Grad↓	Conn↓
Deep Image Matting(DIM) [†]	47.56	0.009	43.29	55.90
HAttMatting [†]	48.98	0.009	41.57	49.93
JIS-c [†]	46.14	0.0079	36.74	40.13
JIS [†]	41.91	0.0080	38.38	39.46
JIH-c [†]	39.33	0.0081	38.48	38.76
JIH [†]	38.52	0.0080	38.23	38.28

Table 3: The quantitative results on Distinctions-646 testset.

thesize 43,100 training images and 1,000 testing images and compare our approach and its ablation study results with AlphaGAN (Lutz, Amliantis, and Smolic 2018), Deep Image Matting (Xu et al. 2017), IndexNet Matting (Lu et al. 2019), AdaMatting (Cai et al. 2019), Learning Based Sampling (Tang et al. 2019), Context-Aware Matting (Hou and Liu 2019), GCA-Matting (Li and Lu 2020), and HDMatt (Yu et al. 2020) in Table 2. In perfect trimap provided situation, Net-M exhibits dominating performance on all four metrics compared with other methods. Also, from ablation study, Net-M possesses three out of four superior metrics except for Gradient error, compared to Net-M without hard mining loss (Net-M-nh) and Net-M without refinement (NLM), which demonstrates effectiveness of each part of our system. In trimap-free case, the comparison between our JI and approaches marked by [†] reveals much more improvement of JI on MSE, Grad, and Conn metrics. In Fig. 5, we represent qualitative comparison between our approaches and other state-of-the-art methods.³ Given additional carefully-prepared trimap, our approach is capable of obtaining more fine-grained details of transparent objects than others do.

³Please refer to supplementary material for visual samples of JI setting.



Figure 6: Ablation comparison of visual results of Joint Inference with Fusion on Distinctions-646 benchmark. From left to right, image, trimap predicted by Net-T, GT, JIS-c, JIS, JIH-c, and JIH.

Distinctions-646 Benchmark: Qiao et al. establish Distinctions-646 dataset, consisting of 646 diversified foreground images (Qiao et al. 2020). Following the same composition rule as AIM, we synthesize 59,600 images for training and 1,000 images for testing. The Table 3 compares our approach with HAttMatting (Qiao et al. 2020) and Deep Image Matting (DIM). Our JI approach with either fusion technique exceeds HAttMatting and Deep Image Matting in SAD and Conn metrics by a solid margin. The Fig. 6 indicates that, after refinement module and the secondary fusion, much deterioration part of coarse matte is removed, which mainly benefits from our semantic-guided network architecture design. Considering a scenario where there is an image whose potential target foreground objects are non-salient or occluded with other equally-conspicuous objects in variegated backgrounds, common trimap-free matting (Zhang et al. 2019; Qiao et al. 2020) that leverages a single RGB image as input is struggling for which object should be extracted. However, our JI strategy smartly decomposes automatic matting into two steps and circumvents this drawback.

Real World Human Data: To demonstrate trimap-free application capability of our approach in real world, we adopt similar adversarial training for real data adaption as Sengupta et al. (Sengupta et al. 2020), in which soft segmentation is generated by Parsing R-CNN (Yang et al. 2019).⁴ We capture 37 handheld videos, in which subject is moving around and camera is moved randomly, and combine them with 10 real-world videos from Background Matting (Sengupta et al. 2020) for training (totally 22,144 real-world video frames). The testset consists of 100 images generated from 10 uniformly-sampled frames of each testing video (totally 10 testing videos, i.e. half self-captured, half Background Matting videos). In user study, we composite matte on black background and compare our approach with Context-Aware Matting. Each user was presented with one web page, showing 100 pairs of original image, composite of ours and CAM with random order of the last two. Participants are asked to rate the left composite relative to the right on three scales, i.e. better, similar, and worse. We survey 10 users and our method achieves 65.8% better, 28.7% simi-

⁴Please refer to supplementary materials for training detail.

Composition-1k testset					
Methods	pixAcc	mIoU Bg	mIoU Unk	mIoU Fg	mIoU
Net-T-20	96.41	93.53	82.78	70.64	82.32
Net-T-30	96.34	93.26	82.57	70.46	82.10
Net-T-40	96.16	92.77	81.74	70.14	81.55
Net-T-50	95.90	92.25	80.58	69.49	80.77
Distinctions-646 testset					
Methods	pixAcc	mIoU Bg	mIoU Unk	mIoU Fg	mIoU
Net-T-20	95.74	96.54	80.83	66.72	81.36
Net-T-30	95.66	96.20	80.22	66.82	81.08
Net-T-40	95.57	96.00	79.60	66.94	80.84
Net-T-50	95.31	95.68	78.34	66.72	80.25

(a) Net-T

Composition-1k testset					Distinctions-646 testset				
Methods	SAD↓	MSE↓	Grad↓	Conn↓	Methods	SAD↓	MSE↓	Grad↓	Conn↓
Late Fusion [†]	58.34	0.011	41.63	59.74	DIM [†]	47.56	0.009	43.29	55.90
HAttMatting [†]	44.01	0.007	29.26	46.41	HAttMatting [†]	48.98	0.009	41.57	49.93
JIS [†] -20	43.91	0.0054	18.64	39.82	JIS [†] -20	41.91	0.0080	38.38	39.46
JIS [†] -30	44.24	0.0055	18.75	40.10	JIS [†] -30	41.96	0.0079	38.38	39.46
JIS [†] -40	44.64	0.0056	18.92	40.43	JIS [†] -40	42.40	0.0079	39.52	39.79
JIS [†] -50	45.55	0.0059	19.47	41.24	JIS [†] -50	43.92	0.0083	40.86	41.27
JIH [†] -20	41.85	0.0055	18.34	39.42	JIH [†] -20	38.52	0.0080	38.23	38.28
JIH [†] -30	42.08	0.0056	18.42	39.66	JIH [†] -30	38.39	0.0078	37.77	38.17
JIH [†] -40	42.29	0.0057	18.53	39.87	JIH [†] -40	38.58	0.0079	38.66	38.37
JIH [†] -50	43.00	0.0060	19.05	40.54	JIH [†] -50	39.88	0.0083	40.27	39.74

(b) JI

Table 4: Comparison of different segmentation inputs for Net-T and JI on different datasets. (<network>-X, like Net-T-X, JIS-X and JIH-X, means that segmentation is generated by erosion on *initial segmentation* from *synthesized ground-truth trimap* with X pixels and followed by a Gaussian Blur.)

lar but only 5.5% worse than CAM, which implies competitive performance of our trimap-free pipeline compared to modest trimap-needed matting on real-world human images with diverse backgrounds. Fig. 7 shows visual comparison. This experiment validates that our approach can be trained to adapt to different domains of soft segmentation, therefore, we are confident about practical value of our pipeline.

Attention block and visualization The Table 5 shows quantitative comparison of the number of parameters and GFLOPs of attention layer(s). Our attention layer is much lighter than that of GCA-Matting in both parameter number and GFLOPs aspects, which shows superiority of our attention. In Fig. 1, we visualize global attention weight map of given image query patch denoted by red box and reconstructed alpha feature A' . The brighter the color is, the larger attention weight (pixel value) the pixel holds. The weights of known and unknown part are shown in the top-left corner of each attention map. It is obvious that our attention module can not only select color-relevant pixels accurately but also capture long-distance pixel-to-pixel relationships. The reorganized alpha feature shown on the right of each row demonstrates that the encoder has already concentrated on unknown areas exquisitely which can promote better feature reconstruction in the decoder.

Ablation study on coarse segmentation input In this section, we present ablation study about coarse foreground segmentation input on Net-T and JI.



Figure 7: Comparison of visual results of real data between CAM and Ours. From left to right, image, CAM and Ours.

Methods	Params	GFLOPs
GCA-Matting	49,792	3.5621
Non-local Matting(Ours)	25,984	0.1416

Table 5: Comparison of the number of parameters and GFLOPs of attention block between our Non-local Matting and GCA-Matting (Li and Lu 2020)

Net-T: We conduct an ablation study to investigate the influence of quality of coarse segmentation on Net-T. We test Net-T with *initial segmentation* eroded by 20, 30, 40, and 50 pixels, which simulates flawed applied circumstances, on Composition-1k and Distinctions-646 testsets as shown in Table 4 (a). The accuracy is all above 90% and the mean IoU of unknown region is fluctuating around 0.80, which implies that Net-T is anti-jamming for unperfect foreground segmentation and capable of offering correct trimap estimation.

JI: To research how segmentation affects trimap-free JI pipeline, we test JIS and JIH with *initial segmentation* eroded by 20, 30, 40, and 50 pixels on Composition-1k and Distinctions-646 testset. The results are illustrated in Table 4 (b). The deviation of each metric is quite slight and most metrics in their worst performance still set a state-of-the-art record, which reveals that our network can still attain robust property when soft segmentation is in an ill-posed state.

Conclusion

In this paper, we propose a novel two-stage trimap-free image matting network, which can predict accurate alpha matte from RGB image and its coarse foreground segmentation. Our matting pipeline can be easily integrated with other state-of-the-art semantic segmentation/salient object detection/matting methods to boost trimap-free matting in real world. Benefiting from semantic information provided by coarse foreground segmentation, our approach employs Trimap Generation Network to capture target objects roughly. The light-weight Non-local Matting Network with Refinement dedicates to transition region under predicted-trimap guidance. Comprehensive experiments indicate that our approach is comparable with state-of-the-art performance on Composition-1k, alphas.matting.com, Distinctions-646 benchmarks, and real imagery in trimap-needed and trimap-free cases.

Acknowledgments

This paper was supported by funding 2019-INT007 from the Shenzhen Institute of Artificial Intelligence and Robotics for Society. Thank Zhixiang Wang, Junjie Hu, and Kangfu Mei for comments.

References

- Aksoy, Y.; Oh, T.-H.; Paris, S.; Pollefeys, M.; and Matusik, W. 2018. Semantic soft segmentation. *ACM Transactions on Graphics (TOG)*, 37(4): 1–13.
- Aksoy, Y.; Ozan Aydin, T.; and Pollefeys, M. 2017. Designing effective inter-pixel information flow for natural image matting. In *Proceedings of the IEEE Conference on Computer Vision and Pattern Recognition*, 29–37.
- Amirul Islam, M.; Kalash, M.; and Bruce, N. D. 2018. Revisiting salient object detection: Simultaneous detection, ranking, and subitizing of multiple salient objects. In *Proceedings of the IEEE Conference on Computer Vision and Pattern Recognition*, 7142–7150.
- Cai, S.; Zhang, X.; Fan, H.; Huang, H.; Liu, J.; Liu, J.; Liu, J.; Wang, J.; and Sun, J. 2019. Disentangled image matting. In *Proceedings of the IEEE International Conference on Computer Vision*, 8819–8828.
- Chen, L.-C.; Papandreou, G.; Schroff, F.; and Adam, H. 2017. Rethinking atrous convolution for semantic image segmentation. *arXiv preprint arXiv:1706.05587*.
- Chen, Q.; Ge, T.; Xu, Y.; Zhang, Z.; Yang, X.; and Gai, K. 2018. Semantic human matting. In *Proceedings of the 26th ACM international conference on Multimedia*, 618–626.
- Chen, Q.; Li, D.; and Tang, C.-K. 2013. KNN matting. *IEEE transactions on pattern analysis and machine intelligence*, 35(9): 2175–2188.
- Chen, Z.; Zheng, Y.; Li, X.; Luo, R.; Jia, W.; Lian, J.; and Li, C. 2020. Interactive trimap generation for digital matting based on single-sample learning. *Electronics*, 9(4): 659.
- Cho, D.; Tai, Y.-W.; and Kweon, I. 2016. Natural image matting using deep convolutional neural networks. In *European Conference on Computer Vision*, 626–643. Springer.
- Chuang, Y.-Y.; Curless, B.; Salesin, D. H.; and Szeliski, R. 2001. A bayesian approach to digital matting. In *Proceedings of the 2001 IEEE Computer Society Conference on Computer Vision and Pattern Recognition. CVPR 2001*, volume 2, II–II. IEEE.
- Dai, Y.; Lu, H.; and Shen, C. 2021. Learning Affinity-Aware Upsampling for Deep Image Matting. In *Proceedings of the IEEE/CVF Conference on Computer Vision and Pattern Recognition*, 6841–6850.
- Deng, Z.; Hu, X.; Zhu, L.; Xu, X.; Qin, J.; Han, G.; and Heng, P.-A. 2018. R3net: Recurrent residual refinement network for saliency detection. In *Proceedings of the 27th International Joint Conference on Artificial Intelligence*, 684–690. AAAI Press.
- Fu, J.; Liu, J.; Tian, H.; Li, Y.; Bao, Y.; Fang, Z.; and Lu, H. 2019. Dual attention network for scene segmentation. In *Proceedings of the IEEE Conference on Computer Vision and Pattern Recognition*, 3146–3154.
- Gastal, E. S.; and Oliveira, M. M. 2010. Shared sampling for real-time alpha matting. In *Computer Graphics Forum*, volume 29, 575–584. Wiley Online Library.
- Grady, L.; Schiwietz, T.; Aharon, S.; and Westermann, R. 2005. Random walks for interactive alpha-matting. In *Proceedings of VIIP*, volume 2005, 423–429.
- Gupta, V.; and Raman, S. 2016. Automatic trimap generation for image matting. In *2016 International Conference on Signal and Information Processing (ICONSIP)*, 1–5. IEEE.
- He, K.; Rhemann, C.; Rother, C.; Tang, X.; and Sun, J. 2011. A global sampling method for alpha matting. In *CVPR 2011*, 2049–2056. IEEE.
- Hou, Q.; and Liu, F. 2019. Context-aware image matting for simultaneous foreground and alpha estimation. In *Proceedings of the IEEE International Conference on Computer Vision*, 4130–4139.
- Hsieh, C.-L.; and Lee, M.-S. 2013. Automatic trimap generation for digital image matting. In *2013 Asia-Pacific Signal and Information Processing Association Annual Summit and Conference*, 1–5. IEEE.
- Huang, Z.; Wang, X.; Huang, L.; Huang, C.; Wei, Y.; and Liu, W. 2019. Ccnet: Criss-cross attention for semantic segmentation. In *Proceedings of the IEEE International Conference on Computer Vision*, 603–612.
- Jetley, S.; Lord, N. A.; Lee, N.; and Torr, P. H. 2018. Learn to pay attention. *arXiv preprint arXiv:1804.02391*.
- Ke, Z.; Li, K.; Zhou, Y.; Wu, Q.; Mao, X.; Yan, Q.; and Lau, R. W. 2020. Is a Green Screen Really Necessary for Real-Time Human Matting? *arXiv preprint arXiv:2011.11961*.
- Lee, P.; and Wu, Y. 2011. Nonlocal matting. In *CVPR 2011*, 2193–2200. IEEE.
- Levin, A.; Lischinski, D.; and Weiss, Y. 2007. A closed-form solution to natural image matting. *IEEE transactions on pattern analysis and machine intelligence*, 30(2): 228–242.
- Levin, A.; Rav-Acha, A.; and Lischinski, D. 2008. Spectral matting. *IEEE transactions on pattern analysis and machine intelligence*, 30(10): 1699–1712.
- Li, J.; Zhang, J.; Maybank, S. J.; and Tao, D. 2020. End-to-end Animal Image Matting. *arXiv preprint arXiv:2010.16188*.
- Li, Y.; and Lu, H. 2020. Natural Image Matting via Guided Contextual Attention. In *Proceedings of the AAAI Conference on Artificial Intelligence*, volume 34, 11450–11457.
- Lin, S.; Ryabtsev, A.; Sengupta, S.; Curless, B. L.; Seitz, S. M.; and Kemelmacher-Shlizerman, I. 2021. Real-time high-resolution background matting. In *Proceedings of the IEEE/CVF Conference on Computer Vision and Pattern Recognition*, 8762–8771.
- Liu, J.; Yao, Y.; Hou, W.; Cui, M.; Xie, X.; Zhang, C.; and Hua, X.-s. 2020. Boosting Semantic Human Matting with Coarse Annotations. In *Proceedings of the IEEE/CVF Conference on Computer Vision and Pattern Recognition*, 8563–8572.

- Lu, H.; Dai, Y.; Shen, C.; and Xu, S. 2019. Indices matter: Learning to index for deep image matting. In *Proceedings of the IEEE International Conference on Computer Vision*, 3266–3275.
- Lutz, S.; Amphianitis, K.; and Smolic, A. 2018. Alphagan: Generative adversarial networks for natural image matting. *arXiv preprint arXiv:1807.10088*.
- Mao, X.; Li, Q.; Xie, H.; Lau, R. Y.; Wang, Z.; and Paul Smolley, S. 2017. Least squares generative adversarial networks. In *Proceedings of the IEEE international conference on computer vision*, 2794–2802.
- Mnih, V.; Heess, N.; Graves, A.; et al. 2014. Recurrent models of visual attention. *Advances in neural information processing systems*, 27: 2204–2212.
- Qian, R. J.; and Sezan, M. I. 1999. Video background replacement without a blue screen. In *Proceedings 1999 International Conference on Image Processing (Cat. 99CH36348)*, volume 4, 143–146 vol.4.
- Qiao, Y.; Liu, Y.; Yang, X.; Zhou, D.; Xu, M.; Zhang, Q.; and Wei, X. 2020. Attention-Guided Hierarchical Structure Aggregation for Image Matting. In *Proceedings of the IEEE/CVF Conference on Computer Vision and Pattern Recognition*, 13676–13685.
- Rhemann, C.; Rother, C.; Wang, J.; Gelautz, M.; Kohli, P.; and Rott, P. 2009. A perceptually motivated online benchmark for image matting. In *2009 IEEE Conference on Computer Vision and Pattern Recognition*, 1826–1833. IEEE.
- Ronneberger, O.; Fischer, P.; and Brox, T. 2015. U-net: Convolutional networks for biomedical image segmentation. In *International Conference on Medical image computing and computer-assisted intervention*, 234–241. Springer.
- Sengupta, S.; Jayaram, V.; Curless, B.; Seitz, S. M.; and Kemelmacher-Shlizerman, I. 2020. Background Matting: The World is Your Green Screen. In *Proceedings of the IEEE/CVF Conference on Computer Vision and Pattern Recognition*, 2291–2300.
- Shahrian, E.; Rajan, D.; Price, B.; and Cohen, S. 2013. Improving image matting using comprehensive sampling sets. In *Proceedings of the IEEE Conference on Computer Vision and Pattern Recognition*, 636–643.
- Shen, X.; Tao, X.; Gao, H.; Zhou, C.; and Jia, J. 2016. Deep automatic portrait matting. In *European conference on computer vision*, 92–107. Springer.
- Shrivastava, A.; Gupta, A.; and Girshick, R. 2016. Training region-based object detectors with online hard example mining. In *Proceedings of the IEEE conference on computer vision and pattern recognition*, 761–769.
- Sun, J.; Jia, J.; Tang, C.-K.; and Shum, H.-Y. 2004. Poisson matting. In *ACM SIGGRAPH 2004 Papers*, 315–321.
- Sun, Y.; Tang, C.-K.; and Tai, Y.-W. 2021. Semantic Image Matting. In *Proceedings of the IEEE/CVF Conference on Computer Vision and Pattern Recognition*, 11120–11129.
- Tang, G.; Müller, M.; Gonzales, A. R.; and Sennrich, R. 2018. Why Self-Attention? A Targeted Evaluation of Neural Machine Translation Architectures. In *Proceedings of the 2018 Conference on Empirical Methods in Natural Language Processing*, 4263–4272.
- Tang, J.; Aksoy, Y.; Oztireli, C.; Gross, M.; and Aydin, T. O. 2019. Learning-based sampling for natural image matting. In *Proceedings of the IEEE Conference on Computer Vision and Pattern Recognition*, 3055–3063.
- Vaswani, A.; Shazeer, N.; Parmar, N.; Uszkoreit, J.; Jones, L.; Gomez, A. N.; Kaiser, Ł.; and Polosukhin, I. 2017. Attention is all you need. In *Advances in neural information processing systems*, 5998–6008.
- Wang, J.; and Cohen, M. F. 2005. An iterative optimization approach for unified image segmentation and matting. In *Tenth IEEE International Conference on Computer Vision (ICCV'05) Volume 1*, volume 2, 936–943. IEEE.
- Wang, J.; and Cohen, M. F. 2007. Optimized color sampling for robust matting. In *2007 IEEE Conference on Computer Vision and Pattern Recognition*, 1–8. IEEE.
- Wang, O.; Finger, J.; Yang, Q.; Davis, J.; and Yang, R. 2007. Automatic natural video matting with depth. In *15th Pacific Conference on Computer Graphics and Applications (PG'07)*, 469–472. IEEE.
- Wang, X.; Girshick, R.; Gupta, A.; and He, K. 2018. Non-local neural networks. In *Proceedings of the IEEE conference on computer vision and pattern recognition*, 7794–7803.
- Wei, T.; Chen, D.; Zhou, W.; Liao, J.; Zhao, H.; Zhang, W.; and Yu, N. 2021. Improved Image Matting via Real-time User Clicks and Uncertainty Estimation. In *Proceedings of the IEEE/CVF Conference on Computer Vision and Pattern Recognition*, 15374–15383.
- Xu, N.; Price, B.; Cohen, S.; and Huang, T. 2017. Deep image matting. In *Proceedings of the IEEE Conference on Computer Vision and Pattern Recognition*, 2970–2979.
- Xu, R.; Li, X.; Zhou, B.; and Loy, C. C. 2019. Deep flow-guided video inpainting. In *Proceedings of the IEEE Conference on Computer Vision and Pattern Recognition*, 3723–3732.
- Yang, L.; Song, Q.; Wang, Z.; and Jiang, M. 2019. Parsing rnn for instance-level human analysis. In *Proceedings of the IEEE Conference on Computer Vision and Pattern Recognition*, 364–373.
- Yu, H.; Xu, N.; Huang, Z.; Zhou, Y.; and Shi, H. 2020. High-Resolution Deep Image Matting. *arXiv preprint arXiv:2009.06613*.
- Zhang, Y.; Gong, L.; Fan, L.; Ren, P.; Huang, Q.; Bao, H.; and Xu, W. 2019. A late fusion CNN for digital matting. In *Proceedings of the IEEE Conference on Computer Vision and Pattern Recognition*, 7469–7478.

Appendices

Introduction

In this supplementary material, we provide our network details, details of soft segmentation generation, and additional matting details and results.

Network Structure Details The Fig. S5, S6, S7, S8, S9, and S10 show our networks in details.

Soft Segmentation Generation Our soft foreground segmentation generation of synthetic datasets is similar to that in Background Matting (Sengupta et al. 2020), which can be found by searching “create_seg” in their github code. Fig. S1 shows code of our soft segmentation process. Besides, the code of our research will be publically available once the paper is accepted.

Matting In this section, we provide matting results and training details.

Adobe Image Matting Benchmark (AIM) The Fig. S2 shows the visual comparison of our approach on JI setting with other matting methods.

AlphaMatting.com Benchmark The submitted methods on this benchmark (Rhemann et al. 2009) are ranked by averaged ranking over 24 alpha matte estimations according to different metrics. In Table S1, our Non-local Matting with Refinement achieves the best SAD result among state-of-the-art methods on the alphamatting.com benchmark at the time of submission as well as satisfactory performance on the other three metrics at the same time. The Table S2, S3 and S4 show MSE, Gradient and Connectivity Error results of several popular methods including ours on alphamatting.com benchmark, which demonstrates promising performance of our approach. Fig. S4 represents visual comparison of our approach and other methods on alphamatting.com benchmark.

Real Data Adaption In this section, details about the real data adaption are provided.

We retrain AIM-pretrained matting pipeline (JI-Real) end-to-end using soft fusion on 22,144 real-world video frames. The Net-T of JI-Real is supervised by pseudo trimap. The pseudo trimap is generated by segmentation (Yang et al. 2019) and then erosion of 15 pixels on the foreground and 50 pixels on the background. The soft segmentation for training is produced by erosion on *initial segmentation* of the pseudo trimap with 20 pixels and followed by a Gaussian Blur. The human-finetuned Net-M serves as a teacher for Net-M of JI-Real. The human-finetuned Net-M means finetuning the AIM-pretrained Net-M on combined human images from AIM and Distinctions-646 datasets by the same setting as Net-M except 0.00004 initial learning rate, 10 batch size, and 100,000 iterations. Both pseudo trimap and human-finetuned Net-M serve as teachers for AIM-pretrained Net-T and Net-M. Soft fusion aggregates these two originally separated networks to an end-to-end trimap-free matting network. The end-to-end training and interaction between generator (matting network) and discriminator help generator jump out of the local minimum of human-finetuned Net-M.

```
##### Training code about Segmentation Generation #####
gt_trimap = cv2.imread(seg_dir + 'gt_trimap.png') #gt_trimap following GCMatting, given ground truth alpha
seg = (trimap * 0).astype(np.float32) #seg is first got by setting unknown and foreground areas to 1, background to 0
self.erosion_kernels = (None) + cv2.getStructuringElement(cv2.MORPH_ELLIPSE, (size, size)) for size in range(1,60)
seg = cv2.erode(seg, self.erosion_kernels(np.random.randint(1, 60)))
seg = cv2.dilate(seg, self.erosion_kernels(np.random.randint(1, 60)))
seg = seg.astype(np.float32)
seg = (255-seg).astype(np.uint8)
k_size_list = [(21,21), (31,31), (41,41)]
seg = cv2.GaussianBlur(seg, seg.astype(np.float32), random.choice(k_size_list), 0)
seg[seg<128] = 0
seg[seg>128] = 1
seg = torch.from_numpy(seg).to(torch.long)
seg = F.one_hot(seg, num_classes=2).permute(2,0,1).float() #convert soft foreground segmentation to 2-channel one
##### Testing code about Segmentation Generation #####
#Below is trimap synthetic method. (Segp to get random version)
fg_mask_gt = (alpha * 1e-5).astype(np.int).astype(np.uint8)
bg_mask_gt = (1 - alpha * 1e-5).astype(np.int).astype(np.uint8)
fg_mask_gt = cv2.erode(fg_mask_gt, self.erosion_kernels[15]) #random version replaces 15 by random variable
bg_mask_gt = cv2.erode(bg_mask_gt, self.erosion_kernels[15]) #random version replaces 15 by random variable
gt_trimap = np.ones_like(alpha) * 128
gt_trimap[fg_mask_gt == 1] = 255
gt_trimap[bg_mask_gt == 1] = 0 #where the synthesized ground-truth trimap is generated.
seg = (trimap * 0).astype(np.float32)
seg = cv2.erode(seg, self.erosion_kernels[erosion_variable]) #erosion_variable can be 20, 30, 40, 50
seg = seg.astype(np.float32)
seg = (255-seg).astype(np.uint8)
seg = cv2.GaussianBlur(seg, seg.astype(np.float32), (31,31), 0) #segmentation is generated
```

Figure S1: Code Snapshot of Soft Foreground Segmentation Generation for Synthetic Datasets

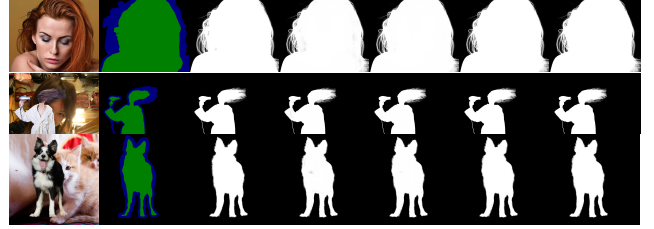


Figure S2: Ablation comparison of visual results of Joint Inference with Fusion on AIM benchmark. From left to right, image, trimap predicted by Net-T, GT, JIS-c, JIH-c, and JIH.

In the joint end-to-end training of JI-Real, we follow almost the same settings as Net-T and Net-M, but the learning rate of Net-T is initialized to 0.0001 and the initial learning rate of 0.00004 for Net-M with 6 batch size, 100,000 iterations, and $L_{coarse.\alpha} + L_{refined.\alpha}$ as the regression loss calculated on the whole image and combined with adversarial loss.

27 background videos are collected, either self-captured or from Background Matting (Sengupta et al. 2020), to provide background images \bar{B} for image composition in training. We use the similar GAN framework and the same configuration of discriminator as Background Matting (Mao et al. 2017; Sengupta et al. 2020) to train our generator, JI-Real, and discriminator D . The overview of real data adaption architecture is shown in Fig. S3. For the generator, we minimize:

$$\min_{\theta_{Real}} E_{X, \bar{B} \sim p_{X, \bar{B}}} [(D(\alpha I + (1 - \alpha)\bar{B}) - 1)^2] + \lambda \{L_{ce} + L_{coarse.\alpha} + L_{refined.\alpha}\}, \quad (6)$$

where $\alpha = \text{JI-Real}(X, \theta_{Real})$, α means the refined alpha matte, X denotes input image I and its coarse segmentation, θ_{Real} is the weights of the JI-Real network, \bar{B} is the given composite background image, λ is 0.5 and reduced by $\frac{1}{2}$ every 10,000 iterations during training, and L_{ce} is the cross-entropy loss of Net-T. For the discriminator, the loss function is

$$\min_{\theta_{Disc}} E_{X, \bar{B} \sim p_{X, \bar{B}}} [(D(\alpha I + (1 - \alpha)\bar{B}))^2] + E_{I \in p_{data}} [(D(I) - 1)^2], \quad (7)$$

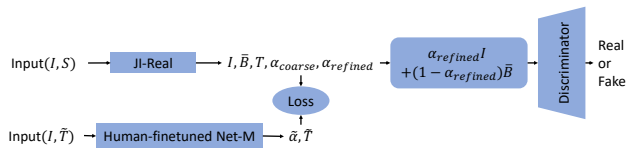


Figure S3: Real Data Adaption Architecture. S is the coarse segmentation of foreground object of image I , \tilde{T} , $\tilde{\alpha}$ are the pseudo trimap and alpha, and $T, \alpha_{coarse}, \alpha_{refined}$ are the predicted trimap, coarse alpha, and refined alpha.

where θ_{Disc} is the weights of the discriminator network.

For CAM testing, we use an image and its corresponding previous-mentioned pseudo trimap as input.

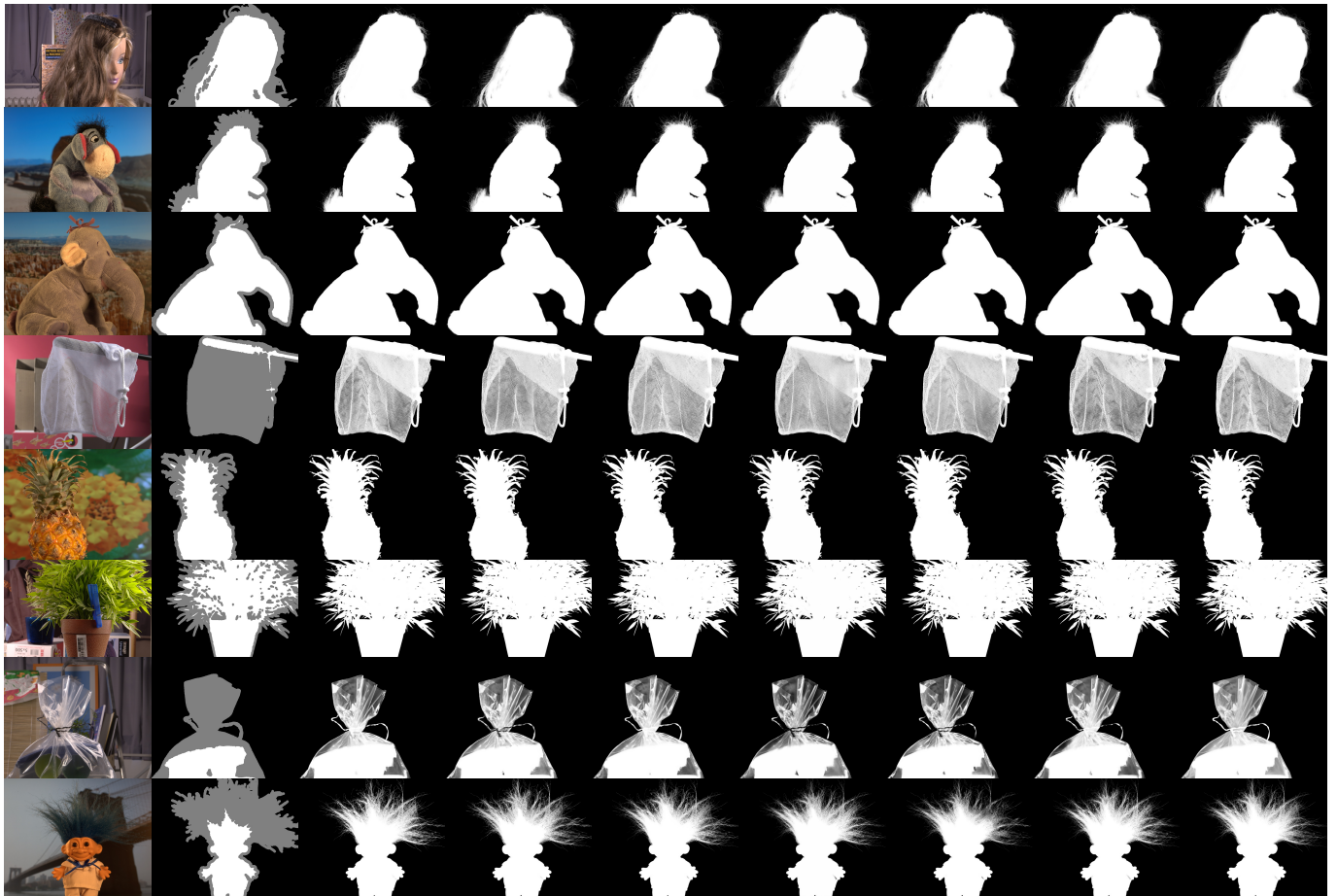


Figure S4: Visual results on alphamattng.com benchmark. From left to right: Image, Trimap (S), HDMatt (Yu et al. 2020), AdaMatting (Cai et al. 2019), GCA Matting (Li and Lu 2020), Context-Aware Matting (Hou and Liu 2019), IndexNet Matting (Lu et al. 2019), SampleNet Matting (Tang et al. 2019), and Non-local Matting with Refinement (Ours).

SAD	Average Rank				Troll			Doll			Donkey			Elephant			Plant			Pineapple			Plastic bag			Net		
	Overall	S	L	U	S	L	U	S	L	U	S	L	U	S	L	U	S	L	U	S	L	U	S	L	U			
HDMatt(Yu et al. 2020)	7.3	9.3	6	6.8	9.5	10	10.7	4.7	4.8	5.8	2.9	3	2.6	1.1	1.2	1.3	5.2	5.9	6.7	2.4	2.6	3.1	17.3	17.3	17	21.5	22.4	23.2
AdaMatting(Cai et al. 2019)	9.1	7.9	8.1	11.4	10.2	11.1	10.8	4.9	5.4	6.6	3.6	3.4	3.4	0.9	0.9	1.8	4.7	6.8	9.3	2.2	2.6	3.3	19.2	19.8	18.7	17.8	19.1	18.6
SampleNet Matting(Tang et al. 2019)	9.5	7.6	9.1	11.9	9.1	9.7	9.8	4.3	4.8	5.1	3.4	3.7	3.2	0.9	1.1	2	5.1	6.8	9.7	2.5	4	3.7	18.6	19.3	19.1	20	21.6	23.2
GCA Matting(Li and Lu 2020)	10.7	11.8	7.9	12.5	8.8	9.5	11.1	4.9	4.8	5.8	3.4	3.7	3.2	1.1	1.2	1.3	5.7	6.9	7.6	2.8	3.1	4.5	18.3	19.2	18.5	20.8	21.7	24.7
Non-local Matting with Refinement(Ours)	6.5	5.8	5.9	8	7	8.1	8.1	4.2	4.4	5.4	2.6	2.6	2.3	1	1	1.2	4.9	5.8	7.6	2.1	2.2	3.2	19.7	22.5	19.9	20.1	20.9	24.7

Table S1: Top-5 SAD results on alphamattng.com benchmark, where S, L, U represent the trimap type of small, large and user, and bold numbers show that our Non-local Matting with Refinement achieves the best SAD performance at the time of submission.

MSE	Average Rank				Troll			Doll			Donkey			Elephant			Plant			Pineapple			Plastic bag			Net		
	Overall	S	L	U	S	L	U	S	L	U	S	L	U	S	L	U	S	L	U	S	L	U	S	L	U			
HDMatt(Yu et al. 2020)	7.5	10.1	6	6.5	0.3	0.3	0.4	0.2	0.2	0.3	0.1	0.1	0.1	0	0	0	0.4	0.4	0.6	0.1	0.2	0.2	0.9	0.9	0.9	0.8	0.8	0.8
AdaMatting(Cai et al. 2019)	9.9	7.6	8.9	13.1	0.3	0.4	0.4	0.2	0.2	0.3	0.2	0.2	0.2	0	0	0.1	0.4	0.6	1	0.1	0.2	0.3	1.1	1.2	1.1	0.6	0.6	0.6
SampleNet Matting(Tang et al. 2019)	10.5	7.1	10.6	13.8	0.3	0.3	0.3	0.1	0.2	0.2	0.2	0.2	0.2	0	0	0.1	0.4	0.6	1.2	0.1	0.3	0.3	1.1	1.1	1.2	0.7	0.8	0.8
GCA Matting(Li and Lu 2020)	11.7	11.6	10.1	13.3	0.3	0.3	0.4	0.2	0.2	0.3	0.2	0.2	0.2	0	0	0.1	0.5	0.6	0.8	0.2	0.2	0.5	1	1.1	1.1	0.7	0.8	0.9
Non-local Matting with Refinement(Ours)	7.5	6.1	7.1	9.4	0.2	0.2	0.3	0.1	0.2	0.2	0.1	0.1	0.1	0	0	0	0.4	0.5	0.8	0.1	0.1	0.3	1.1	1.3	1.1	0.7	0.8	0.9

Table S2: Top-5 MSE results on AlphaMatting benchmark, S, L, U represent the trimap type of small, large and user at the time of submission.

Gradient	Average Rank				Troll			Doll			Donkey			Elephant			Plant			Pineapple			Plastic bag			Net		
	Overall	S	L	U	S	L	U	S	L	U	S	L	U	S	L	U	S	L	U	S	L	U	S	L	U			
HDMatt(Yu et al. 2020)	5.6	6.5	4	6.4	0.2	0.2	0.2	0.1	0.1	0.3	0.1	0.1	0.2	0.2	0.2	0.3	1.1	1.2	1.6	0.6	0.6	0.9	0.5	0.5	0.6	0.3	0.4	0.4
AdaMatting(Cai et al. 2019)	9.4	5.9	7	15.4	0.2	0.2	0.2	0.1	0.1	0.4	0.2	0.2	0.2	0.1	0.1	0.3	1.1	1.4	2.3	0.4	0.6	0.9	0.9	1	0.9	0.3	0.4	0.4
GCA Matting(Li and Lu 2020)	9.7	9.9	8.1	11	0.1	0.1	0.2	0.1	0.1	0.3	0.2	0.2	0.2	0.2	0.2	0.3	1.3	1.6	1.9	0.7	0.8	1.4	0.6	0.7	0.6	0.4	0.4	0.4
Context-aware Matting(Hou and Liu 2019)	10.9	12.4	11.6	8.6	0.2	0.2	0.2	0.1	0.2	0.2	0.2	0.2	0.2	0.2	0.4	0.4	1.4	1.5	1.8	0.8	1.3	1	1.1	1.1	0.9	0.4	0.4	0.4
Non-local Matting with Refinement(Ours)	6.7	5.6	5.5	8.9	0.2	0.2	0.2	0.1	0.1	0.2	0.1	0.1	0.2	0.2	0.2	0.3	1	1.3	2	0.5	0.5	1	0.5	0.5	0.5	0.4	0.5	0.4

Table S3: Top-5 Gradient results on AlphaMatting benchmark, S, L, U represent the trimap type of small, large and user at the time of submission.

Connectivity Error	Average Rank				Troll			Doll			Donkey			Elephant			Plant			Pineapple			Plastic bag			Net		
	Overall	S	L	U	S	L	U	S	L	U	S	L	U	S	L	U	S	L	U	S	L	U	S	L	U			
GCA Matting(Li and Lu 2020)	19.7	22.9	17.3	18.9	1.1	1.1	1	0.2	0.2	0.2	0.2	0.2	0.2	0	0	0	0.1	0.1	0.1	0	0.1	0.1	1.1	1.3	1.3	1.9	1.5	1.6
AdaMatting(Cai et al. 2019)	21	19	23.1	20.8	1.1	1.1	1.1	0.1	0.2	0.2	0.2	0.2	0.2	0	0	0	0.1	0.1	0.1	0	0	0.1	6.8	13.3	1.4	1.3	1.3	1.3
IndexNet Matting(Lu et al. 2019)	23.1	21.7	24.5	23	1.3	1.3	1.3	0.1	0.1	0.1	0.2	0.2	0.2	0	0	0	0.1	0.1	0.3	0	0.1	0.2	10	10.7	1.8	1.6	1.7	1.6
SampleNet Matting(Tang et al. 2019)	23.4	25	21	24.5	0.9	0.9	0.8	0.1	0.1	0.1	0.2	0.2	0.2	0	0	0	0.1	0.1	0.2	0	0.1	0.2	1.5	1.5	1.8	3.8	3.9	3.8
Non-local Matting with Refinement(Ours)	17.3	19.7	14.7	17.4	0.9	0.9	0.9	0.1	0.1	0.1	0.2	0.2	0.2	0	0	0	0.1	0.1	0.2	0	0	0	0.9	0.7	0.9	3.2	3.3	3.2

Table S4: Popular matting approach results of Connectivity Error on AlphaMatting benchmark, S, L, U represent the trimap type of small, large and user at the time of submission.

Block Name	Output Size	Details
Encoder		
Conv+BN+ReLU	$256 \times 256 \times 64$	7×7 , 64, stride 2, Bias=False
Layer1	$128 \times 128 \times 256$	3×3 max pool, stride=2; Block $\times 3$, stride=[1,1,1], atrous=[1,1,1]
Layer2	$64 \times 64 \times 512$	Block $\times 4$, stride=[2,1,1,1], atrous=[1,1,1,1]
Layer3	$32 \times 32 \times 1024$	Block $\times 6$, stride=[2,1,1,1,1,1], atrous=[1,1,1,1,1,1]
Layer4	$32 \times 32 \times 2048$	Block $\times 3$, stride=[1,1,1], atrous=[1,2,1]
Decoder		
ASPP+Dropout	$32 \times 32 \times 256$	rate of ASPP=1, dropout ratio=0.5; input: output of Layer4
Layer1-Shortcut(Conv2+BN+ReLU)	$128 \times 128 \times 48$	1×1 , 48, stride=1, Bias=True; input: output of Layer1
Layer2-Shortcut (Conv3+BN+ReLU)	$128 \times 128 \times 48$	1×1 , 48, stride=1, Bias=True; input: 2×2 bilinear upsampling from Layer2
Concatenation Conv (Conv4+BN+ReLU+ Dropout+Conv5+BN+ ReLU+Dropout)	$128 \times 128 \times 48$	3×3 , 256, stride=1, Bias=True; 3×3 , 256, stride 1, Bias=True; Dropout ratio=0.1; input: concatenation of 4×4 bilinear upsampling from ASPP+Dropout, output of Layer2-Shortcut and Layer1-Shortcut
Output Conv (Conv6)	$512 \times 512 \times 3$	1×1 , 3, stride=1, Bias=True; input: 4×4 bilinear upsampling from Concatenation Conv

Figure S5: Trimap Generation Network. Block is the Bottleneck of ResNet-atrous from <https://download.pytorch.org/models/resnet50-19c8e357.pth>

Block Name	Output Size	Details
Encoder		
Stride Conv1+SN+BN	$256 \times 256 \times 32$	$3 \times 3, 32, \text{stride } 2, \text{Bias}=\text{False}$
ShortCut1($2*(\text{Conv}+\text{SN}+\text{ReLU}+\text{BN})$)	$512 \times 512 \times 32$	$3 \times 3, 32, \text{stride}=1, \text{Bias}=\text{False}; \text{input: original image}$
Conv1+SN+BN	$256 \times 256 \times 32$	$3 \times 3, 32, \text{stride } 1, \text{Bias}=\text{False}$
ShortCut2($2*(\text{Conv}+\text{SN}+\text{ReLU}+\text{BN})$)	$256 \times 256 \times 32$	$3 \times 3, 32, \text{stride}=1, \text{Bias}=\text{False}; \text{input: output of Conv1+SN+BN}$
Stride Conv2+SN+BN	$128 \times 128 \times 64$	$3 \times 3, 64, \text{stride } 2, \text{Bias}=\text{False}; \text{input: output of Conv1+SN+BN}$
ResBlocks1	$128 \times 128 \times 64$	Block \times 3, stride=[1,1,1]
ShortCut3($2*(\text{Conv}+\text{SN}+\text{ReLU}+\text{BN})$)	$128 \times 128 \times 64$	$3 \times 3, 64, \text{stride}=1, \text{Bias}=\text{False}; \text{input: output of ResBlocks1}$
Downsample ResBlock1	$64 \times 64 \times 128$	Block \times 1, stride=[2]
ResBlocks2	$64 \times 64 \times 128$	Block \times 3, stride=[1,1,1]
Non-local Block	$64 \times 64 \times 128$	input: image and alpha feature from ResBlocks2
ShortCut4($2*(\text{Conv}+\text{SN}+\text{ReLU}+\text{BN})$)	$64 \times 64 \times 128$	$3 \times 3, 128, \text{stride}=1, \text{Bias}=\text{False}; \text{input: output of Non-local Block}$
Downsample ResBlock2	$32 \times 32 \times 256$	Block \times 1, stride=[2]
ResBlocks2	$32 \times 32 \times 256$	Block \times 3, stride=[1,1,1]
ShortCut5($2*(\text{Conv}+\text{SN}+\text{ReLU}+\text{BN})$)	$32 \times 32 \times 256$	$3 \times 3, 256, \text{stride}=1, \text{Bias}=\text{False}; \text{input: output of ResBlocks2}$
Downsample ResBlock3	$16 \times 16 \times 512$	Block \times 1, stride=[2]
ResBlock3	$16 \times 16 \times 512$	Block \times 1, stride=[1]
Decoder		
Upsample ResBlock1	$32 \times 32 \times 256$	Block \times 1, stride=[2]
ResBlocks4	$32 \times 32 \times 256$	Block \times 1, stride=[1]
Upsample ResBlock2	$64 \times 64 \times 128$	Block \times 1, stride=[2]; input: the summation of output of ShortCut5 and ResBlocks4
ResBlocks5	$64 \times 64 \times 128$	Block \times 2, stride=[1,1]
Upsample ResBlock3	$128 \times 128 \times 64$	Block \times 1, stride=[2]; input: the summation of output of ShortCut4 and ResBlocks5
ResBlocks6	$128 \times 128 \times 64$	Block \times 2, stride=[1,1]
Upsample ResBlock4	$256 \times 256 \times 32$	Block \times 1, stride=[2]; input: the summation of output of ShortCut3 and ResBlocks6
ResBlocks7	$256 \times 256 \times 32$	Block \times 1, stride=[1]
Deconv1+SN+BN	$512 \times 512 \times 32$	$4 \times 4, 32, \text{stride}=2, \text{bias}=\text{False}; \text{input: the summation of output of ShortCut2 and ResBlocks7}$
Conv2+SN+BN	$512 \times 512 \times 1$	$3 \times 3, 1, \text{stride}=1, \text{bias}=\text{True}; \text{input: the summation of output of ShortCut1 and Deconv1+SN+BN}$

Figure S6: Non-local Matting. ResBlock, ResBlock with downsampling and upsampling are shown in following figures.

Block Name	Details
Conv1+SN+BN+ReLU	$3 \times 3, \text{stride}=1, \text{bias}=\text{False}$
Conv2+SN+BN	$3 \times 3, \text{stride}=1, \text{bias}=\text{False}$
ReLU	input: the summation of original block input and output of Conv2+SN+BN

Figure S7: ResBlock in Encode. In the decoder, ReLU is replaced with LeakyReLU.

Block Name	Details
Conv1+SN+BN+ReLU	3×3 , stride=2, bias=False
Conv2+SN+BN	3×3 , stride=1, bias=False
Downsampling Layer	2×2 Avg Pool; input: original block input
ReLU	input: the summation of output of Downsampling Layer and Conv2+SN+BN

Figure S8: ResBlock with Downsampling

Block Name	Details
DeConv1+SN+BN+LeakyReLU	4×4 , stride=2, bias=False
Conv2+SN+BN	3×3 , stride=1, bias=False
Upsampling Layer	Nearest Upsampling; input: original block input
LeakyReLU	input: the summation of output of Upsampling Layer and Conv2+SN+BN

Figure S9: ResBlock with Upsampling

Block Name	Output Size	Details
Encoder		
Conv0	$512 \times 512 \times 1$	3×3 , 1, stride=1, Bias=True
Conv1+BN+ReLU+MaxPool	$256 \times 256 \times 64$	3×3 , 64, stride=1, Bias=True; 2×2 Max Pool
Conv2+BN+ReLU+MaxPool	$128 \times 128 \times 64$	3×3 , 64, stride=1, Bias=True; 2×2 Max Pool
Conv3+BN+ReLU+MaxPool	$64 \times 64 \times 64$	3×3 , 64, stride=1, Bias=True; 2×2 Max Pool
Conv4+BN+ReLU+MaxPool	$32 \times 32 \times 64$	3×3 , 64, stride=1, Bias=True; 2×2 Max Pool
Decoder		
Conv5+BN+ReLU+Upsample	$64 \times 64 \times 64$	3×3 , 64, stride=1, Bias=True; 2×2 bilinear upsampling; input: output of Conv4+BN+ReLU+MaxPool
Conv6+BN+ReLU+Upsample	$128 \times 128 \times 64$	3×3 , 64, stride=1, Bias=True; 2×2 bilinear upsampling; input: concatnation of output of Conv5+BN+ReLU+Upsample and Conv4+BN+ReLU+MaxPool
Conv7+BN+ReLU+Upsample	$256 \times 256 \times 64$	3×3 , 64, stride=1, Bias=True; 2×2 bilinear upsampling; input: concatnation of output of Conv6+BN+ReLU+Upsample and Conv3+BN+ReLU+MaxPool
Conv8+BN+ReLU+Upsample	$512 \times 512 \times 64$	3×3 , 64, stride=1, Bias=True; 2×2 bilinear upsampling; input: concatnation of output of Conv7+BN+ReLU+Upsample and Conv2+BN+ReLU+MaxPool
Conv9+BN+ReLU	$512 \times 512 \times 64$	3×3 , 64, stride=1, Bias=True; 2×2 bilinear upsampling; input: concatnation of output of Conv8+BN+ReLU+Upsample and Conv1+BN+ReLU+MaxPool
Conv10	$512 \times 512 \times 1$	3×3 , stride=1, bias=True; input: output of Conv9+BN+ReLU
Residual	$512 \times 512 \times 1$	summation of output of Conv10 and original network input coarse alpha

Figure S10: Refinement Module